Preparation and magnetic properties of nickel nanoparticles via the thermal decomposition of nickel organometallic precursor in alkylamines

2007 Nanotechnology 18 505703

(http://iopscience.iop.org/0957-4484/18/50/505703)

IOP PUBLISHING NANOTECHNOLOGY
Nanotechnology **18** (2007) 505703 (6pp) doi:10.1088/0957-4484/18/50/505703

Preparation and magnetic properties of nickel nanoparticles via the thermal decomposition of nickel organometallic precursor in alkylamines

Yuanzhi Chen, Dong-Liang Peng, Dongxing Lin and Xiaohua Luo

Department of Materials Science and Engineering, College of Chemistry and Chemical Engineering, Xiamen University, Xiamen 361005, People's Republic of China

E-mail: dlpeng@xmu.edu.cn

Received 8 August 2007, in final form 19 October 2007
Published 20 November 2007
Online at stacks.iop.org/Nano/18/505703

Abstract
Nickel nanoparticles were prepared from the thermal decomposition of nickel(II) acetylacetonate in alkylamines and characterized by powder x-ray diffraction, transmission electron microscopy and magnetic measurement. The reaction temperature, heating rate and solvent type play an important role in the control over the crystalline phase. Depending on the reaction conditions, face-centered cubic (fcc) or hexagonal close-packed (hcp) nickel nanoparticles can be obtained. Monodisperse nickel nanoparticles were also obtained by introducing surfactants. The results of magnetic characterization showed that the magnetic properties of the hcp nickel nanoparticles are quite different from those of the fcc nickel nanoparticles.

1. Introduction

The study of metal nanoparticles has been an extremely active research area in the past decade. Due to their small dimensions and large specific surface areas, metal nanoparticles often exhibit novel material properties that differ considerably from those of the bulk materials [1–3]. In order to take maximum advantage of those novel properties which are often affected by particle size, shape and crystalline phase, synthetic protocols are needed in which significant control can be exercised over those parameters. Numerous physical and chemical methods have been used to produce metal nanoparticles, such as metal evaporation–condensation, electrochemical methods, sonochemical synthesis, metal salt reduction and neutral organometallic precursor decomposition. Generally, chemical synthesis methods have the advantages of simplicity and low cost compared with physical approaches.

Nickel nanoparticles have attracted much attention because of their use in numerous practical applications, such as magnetic materials, conducting materials and catalysts. As a result, various approaches have been developed to prepare high-quality nickel nanoparticles, especially the solution-phase chemistry routes [4–22], which provide facile and diverse ways to achieve the control over particle size, morphology and crystalline phase.

Among the various solution-phase chemistry routes developed for preparation of nickel nanoparticles, the reduction of metal salts is the most common, and reducing agents such as $NaBH_4$ [5, 6], hydrazine [8–11] and polyols [4, 12–15] have been commonly employed in the reactions. Recent studies have shown that amine can be used as a mild reducing agent or ligand to obtain the metallic forms of metal elements from their inorganic or organic salts. For instance, monodisperse gold and silver nanoparticles have been successfully prepared in a reaction system containing alkylamines [23, 24]. Although nickel is more difficult to be reduced compared to noble metals, recent studies have shown that nickel nanoparticles can also be produced from the direct decomposition of nickel organometallic precursor in some alkylamines such as oleylamine [16, 17] and dodecylamine [18]. However, the full formation mechanism of nickel nanoparticles is still not clear at present and the simultaneous control over particle size and crystalline phase in one-pot synthesis is also not easy to achieve. Nevertheless, employing appropriate amines as both solvents and reducing agents not only simplifies the preparation process

but also provides an interesting route to prepare high-quality nanocrystals of controlled structure, size and morphology.

The aim of this work is to explore the influences of the reaction parameters on the preparation of nickel nanoparticles by using a synthetic protocol that uses alkylamines as both the solvents and reducing agents, wherein a nickel organometallic precursor (nickel(II) acetylacetonate) is thermally decomposed to generate nickel nanoparticles. We will show that the quality of the obtained nickel nanoparticles is related to the reaction temperature, heating rate, solvent type and, to some extent, the choice of surfactant. By manipulating these reaction parameters, we are able to control the crystalline phase and particle size distribution. Finally, we compare the magnetic properties of the as-synthesized face-centered cubic (fcc) and the hexagonal close-packed (hcp) nickel nanoparticles.

2. Experimental section

2.1. Synthesis

Nickel(II) acetylacetonate ($Ni(acac)_2$, 95%, Alfa Aesar) was used as an organometallic precursor to synthesize nickel nanoparticles in this study. In a typical reaction, 1 mmol of $Ni(acac)_2$ was added to 7 ml of an alkylamine (e.g. oleylamine) and the mixture was stirred magnetically under a flow of high-purity argon gas at room temperature for 20 min. The alkylamines used in this study include oleylamine (70%, Fluka), tri-n-octylamine (98%, Alfa Aesar), dodecylamine (commercial C.P. grade) and hexadecylamine (90%, Acros). The mixture was further heated to 130 °C and maintained for 20 min. The mixture was then rapidly heated to the designed temperature (215–285 °C) and kept at that temperature for an additional 30 min. Reaction temperature and time could be varied to obtain the desired results. After cooling to room temperature, 20 ml of ethanol was added to the solution to give a black precipitate, which was separated from the solution by centrifugation. The obtained nanoparticles were further washed and separated by repeated precipitation of the mixture of hexane and ethanol and dried in a vacuum.

2.2. Characterization

Powder x-ray diffraction (XRD) patterns of the as-synthesized nickel nanoparticles were recorded using a Panalytical X'pert PRO x-ray diffractometer with Cu Kα radiation. Transmission electron microscopy (TEM) was performed on a TECNAI F-30 transmission electron microscope operating at 300 kV. Selected-area electron diffraction (SAED) was used to identify the crystalline phases. Samples for TEM examination were prepared by placing a drop of the sample suspension on a copper grid coated with a carbon film and was allowed to dry in air. Magnetic measurements were carried out with a superconducting quantum interference device (SQUID) magnetometer (MPMS-5) in a temperature range of 5–300 K.

3. Results and discussion

3.1. Structural characterization

Figure 1 shows the XRD patterns of nickel nanoparticles produced by the thermal decomposition of $Ni(acac)_2$ in oleylamine within 30 min at a temperature of 215 °C, 245 °C and 260 °C, respectively. All these samples show crystalline characteristics revealing by distinctive diffraction peaks. The XRD pattern of the sample synthesized at 215 °C (figure 1(a)) exhibits three characteristic peaks corresponding to the (111), (200) and (220) lattice planes of fcc nickel. No characteristic peaks of crystalline nickel oxides have appeared, probably owing to the protecting effect of oleylamine covering the particle surfaces. Increasing the reaction temperature to 240 °C apparently did not result in a change of the crystalline phase (figure 1(b)). This outcome is similar to that reported in a previous study [16], in which fcc nickel nanoparticles were also obtained by using the same starting materials at the same reaction temperature.

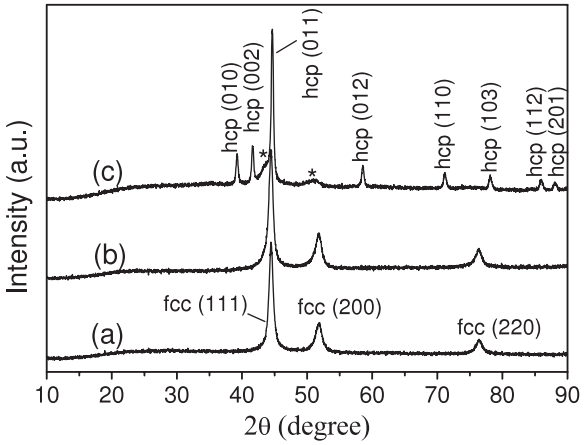

Figure 1. XRD patterns of nickel nanoparticles produced by the thermal decomposition of $Ni(acac)_2$ in oleylamine at 215 °C (a), 240 °C (b) and 260 °C (c), respectively. The asterisks in sample (c) represent unidentified phases.

However, when the reaction temperature was raised to 260 °C, the hcp crystalline structure was observed, as evidenced from the XRD pattern shown in figure 1(c). The result indicates that the transition from the fcc to the hcp phase occurs in a narrow temperature range between 240 and 260 °C. In addition, weak diffraction peaks ($2\theta = 43.6$ and 50.6) that do not belong to the hcp phase also appear in the XRD pattern (marked by the asterisks in figure 1(c)). Such peaks could be indexed to a cubic phase whose lattice is slightly larger than that of ideal nickel. One of the possible explanations for such peaks is the lattice increase of fcc nickel, which may involve the diffusion of carbon atoms into the lattice of nickel. However accurate identification of such a crystalline phase needs further studies.

It is worth mentioning that, in a recent study on the preparation of nickel nanoparticles in polyethylene glycols, hcp nickel nanoparticles were also obtained at a higher temperature [15]. Such a temperature-dependence behavior is similar to the one observed in this study, though the starting materials and the reaction conditions are different. The formation of the hcp phase occurring at a higher reaction temperature certainly relates to thermodynamic factors. Since an elevated temperature promotes a faster decomposition of nickel precursor and produces a higher concentration of nickel atoms, which may be thermodynamically favorable for the

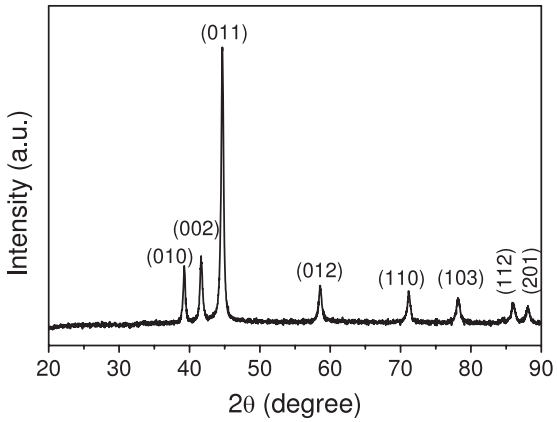

Figure 2. An XRD pattern of the hcp nickel nanoparticles produced by the thermal decomposition of $Ni(acac)_2$ in the mixture of oleylamine and octadecene at 240 °C.

formation of the hcp phase. On the other hand, it also has connections with kinetic factors because we found that the formation of the hcp phase was sensitive to the heating rate during the reaction. When a slow heating rate of 3 °C min^{-1} was used to reach the reaction temperature of 260 °C, the crystalline phase would remain the fcc phase. This indicates that both thermodynamic and kinetic factors were involved in the formation of the metastable hcp phase. However, the involved full formation mechanism still needs further studies. Further increasing the reaction temperature to 285 °C would still generate hcp nickel nanoparticles, coexisting with small amounts of impurities, probably nickel carbides.

The above results demonstrate that the phase control of nickel nanoparticles can be roughly achieved by adjusting the reaction temperature and heating rate. As discussed above, the sample synthesized in pure oleylamine at 260 °C contains the dominant hcp nickel plus small amounts of impurities which may have influences on its magnetic properties. In order to obtain the pure hcp nickel nanoparticles, strict control over the reaction temperature and heating rate are needed, which may bring difficulties for the experiment. Therefore, we adjusted the synthetic route wherein the $Ni(acac)_2$ was decomposed in the mixture of oleylamine (3 mmol) and octadecene (7 ml) at a temperature of 240 °C for 45 min. Figure 2 shows the XRD pattern of the obtained products. All the diffraction peaks can be indexed to hcp nickel and no other impurity peaks is observed, hence confirming the formation of the pure hcp crystalline phase. The formation of the pure hcp phase is also reflected in the results of magnetic measurement that will be discussed in the next section.

Figure 3 shows typical TEM images of the as-synthesized fcc and hcp nickel nanoparticles respectively. The fcc nickel nanoparticles synthesized in pure oleylamine at 215 °C exhibit a rather broad size distribution in the range of 10–50 nm. The particles have near-spherical or irregular shaped morphologies. The hcp nickel nanoparticles synthesized in the mixture of oleylamine and octadecene at 240 °C also exhibit polydispersed nanocrystals in the size range of 25–50 nm. Particles having near-cubic or multiangular morphologies are typical in the TEM image.

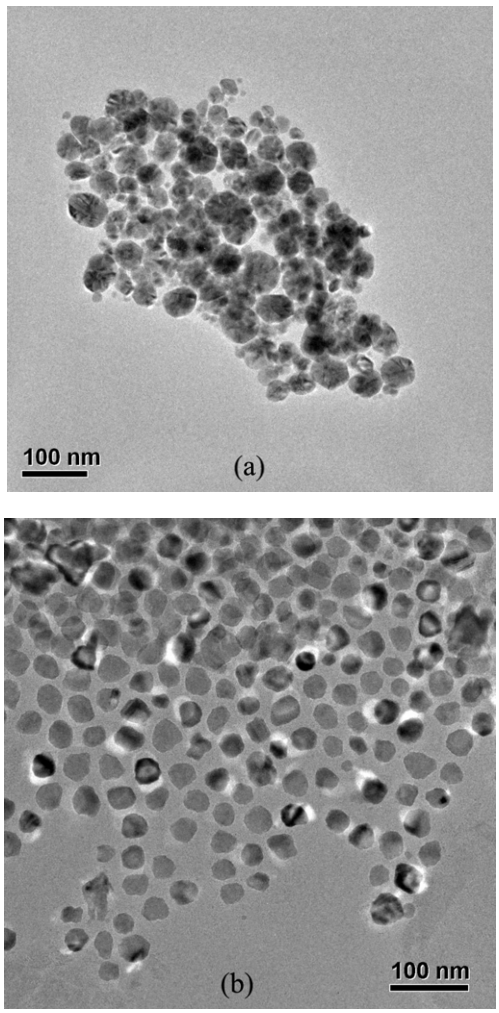

Figure 3. (a) A TEM image of the fcc nickel nanoparticles produced in oleylamine at 215 °C. (b) A TEM image of the hcp nickel nanoparticles produced in the mixture of oleylamine and octadecene at 240 °C.

We also performed experiments on the thermolysis of $Ni(acac)_2$ in other alkylamines, including tri-n-octylamine (TOA), dodecylamine (DDA) and hexadecylamine (HDA). The sample produced in TOA at 260 °C for 30 min exhibited a XRD pattern having mostly fcc nickel peaks plus weak peaks belonging to hcp nickel (figure 4(a)). Such a result is somewhat different from that obtained in oleylamine at the same reaction temperature within the same time window. This may relate to the more bulky structure of the trioctyl groups of TOA, which may inhibit the phase transition of the nickel nanoparticles. Increasing the reaction temperature to 285 °C significantly increased the relative amounts of the hcp phase (figure 4(b)), though small amounts of the fcc phase were still preserved. Interestingly, no other impurity phases were identified in the XRD pattern. When the thermolysis temperature was set to 245 °C, the synthesized products in TOA also showed a similar XRD pattern to that obtained at 260 °C. However, further decreasing the temperature to 215 °C could not lead to the notable decomposition of $Ni(acac)_2$ in the chosen time window of 30 min.

The decomposed products of $Ni(acac)_2$ in DDA follow a similar trend to those produced in oleylamine. As shown

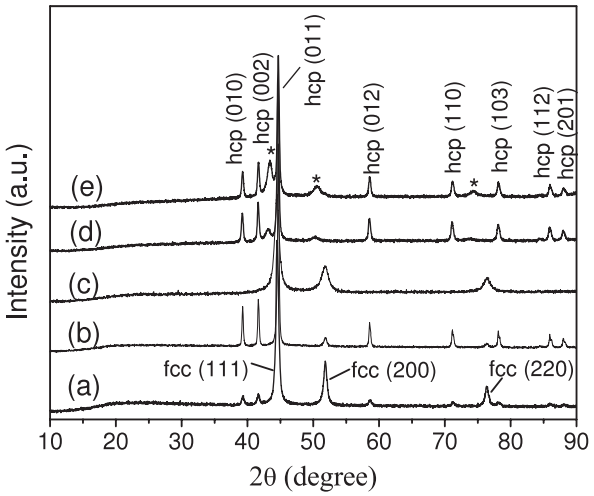

Figure 4. XRD patterns of nickel nanoparticles produced by the thermal decomposition of $Ni(acac)_2$ in tri-n-octylamine at 260 °C (a), tri-n-octylamine at 285 °C (b), dodecylamine at 215 °C (c), dodecylamine at 280 °C (d), and hexadecylamine at 280 °C (e), respectively. The asterisks in sample (e) represent unidentified phases.

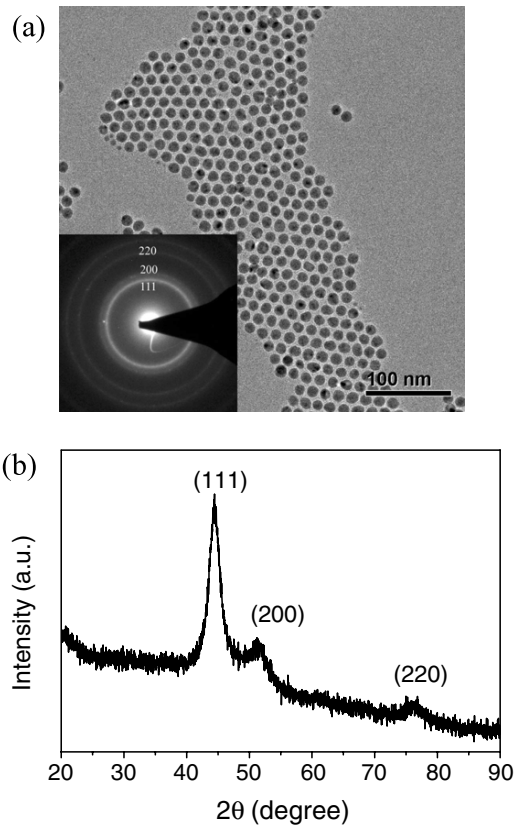

Figure 5. (a) A TEM image of the as-synthesized monodisperse nickel nanoparticles with a mean diameter of 12.9 nm. Inset is the SAED pattern indexed to fcc nickel. (b) An XRD pattern of the nickel nanoparticles shown in (a).

in figures 4(c) and (d), the products synthesized in DDA at 215 °C have the fcc phase, whereas those synthesized at a higher temperature, i.e. 280 °C, possess predominantly the hcp phase. The presence of an impurity phase at a higher reaction temperature is also evidenced from the XRD pattern. The decomposition behavior of $Ni(acac)_2$ in HDA is similar to that in DDA. The formation of the hcp phase has been observed at a higher reaction temperature (figure 4(e)). These results indicate that the formation of the hcp phase favors a higher reaction temperature in these chosen alkylamines.

TEM analyses of the samples synthesized in TOA and DDA and HDA showed that the particles exhibited broad size distributions with typical particle sizes varying from 30 to 60 nm and typically possessed near-spherical or irregular shaped morphologies. Although the particle size and morphology could be adjusted to some extent by controlling the reaction temperature and heating rate, monodisperse nanoparticles could not be obtained in these pure alkylamines. Therefore, we tried to introduce two surfactants, i.e. oleic acid and trioctylphosphine (TOP), into the reaction systems to study their influences on the nickel nanoparticles.

We found that the addition of small amounts of oleic acid (1–3 mmol) into the reaction system still could not lead to the formation of monodisperse nickel nanoparticles. However, the presence of oleic acid delayed the transformation of the fcc phase into the hcp phase. For instance, the product obtained in the presence of 3 mmol oleic acid in 7 ml oleylamine at 260 °C still possessed the fcc phase whereas that obtained in pure oleylamine at the same temperature already transformed into the hcp phase. When small amounts of TOP were added into the reaction systems, the particle size distribution and morphology were well controlled. As shown in figure 5(a), nanoparticles synthesized in the presence of 1 mmol TOP plus 2 mmol oleic acid using oleylamine as solvent at 245 °C possess a spherical morphology and a highly narrow particle size distribution with a mean particle diameter of 12.9 nm. These monodisperse nickel nanoparticles are also organized in a compact hexagonal network. The formation of such a self-assembled two-dimensional monolayer is due to the high uniformity of these nanoparticles and the surfactants covered on the particle surfaces, which separate each particle from agglomerating. The SAED pattern (figure 5(a) inset) obtained from these nanoparticles reveals a crystalline structure corresponding to fcc nickel. The XRD pattern of this sample also exhibits three diffraction peaks indexed to fcc nickel (figure 5(b)). Interestingly, when the reaction temperature was set to above 260 °C (e.g. 280 °C), the crystalline phase of these monodisperse nickel nanoparticles would remain the fcc type, and no transition to the hcp phase was observed. This indicates that surfactants also play an important role in the phase control of the nickel nanoparticles. Further studies are underway on the effects of surfactant types and concentrations on the preparation of monodisperse nickel nanoparticles in alkylamine systems.

3.2. Magnetic characterization

The magnetic properties of the as-synthesized nickel nanoparticles were studied by measuring both the temperature-dependent magnetization (M–T) and hysteresis (M–H) curves. For the zero-field-cooled (ZFC) measurement, the sample was cooled to 5 K in the absence of an external magnetic

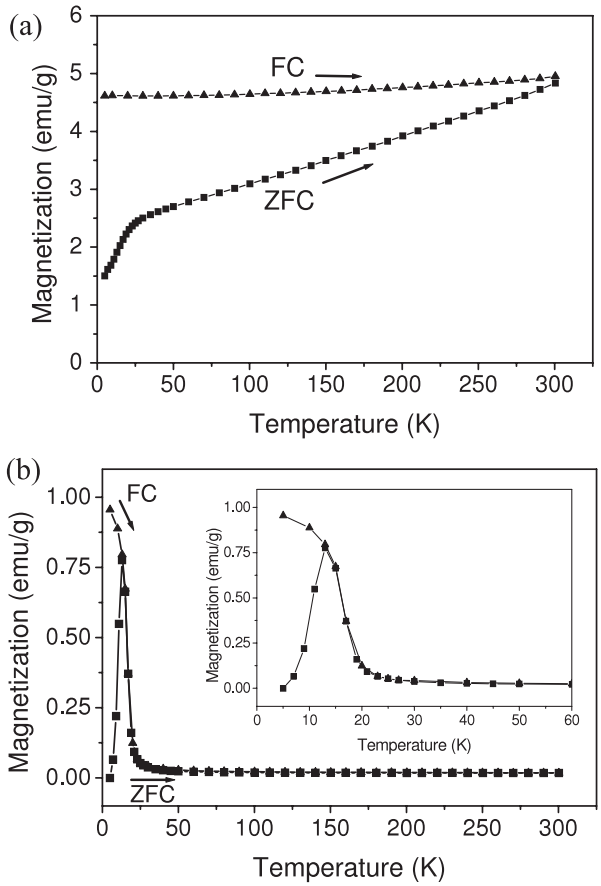

Figure 6. Zero-field-cooled (ZFC) (■) and field-cooled (FC) (▲) magnetization versus temperature curves for fcc nickel nanoparticles (a) and hcp nickel nanoparticles (b). The field applied for magnetization was 100 Oe.

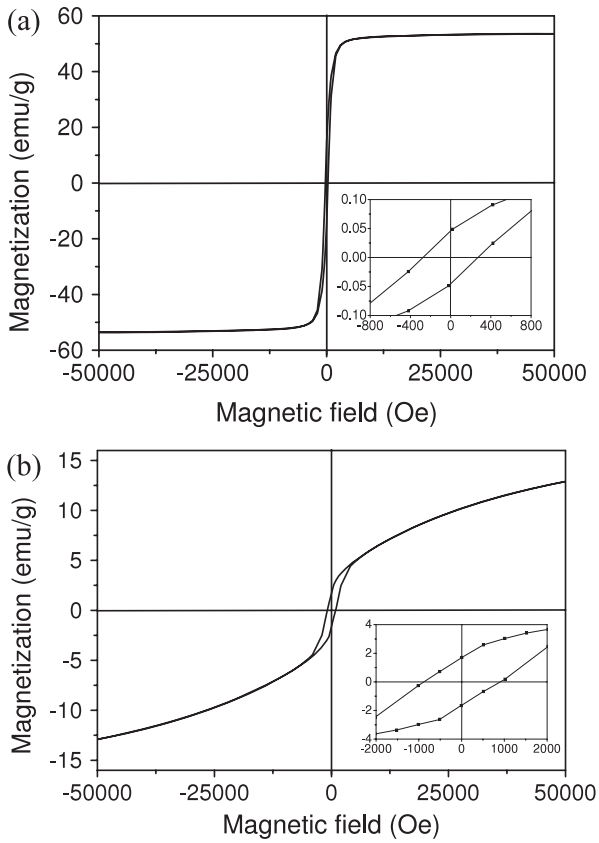

Figure 7. Magnetization versus applied field hysteresis loops measured at 5 K for fcc nickel nanoparticles (a) and hcp nickel nanoparticles (b). The insets show the low field detail of the cycles.

field. A field of 100 Oe was then applied and the magnetization was measured with increasing temperature. For the field-cooled (FC) measurement, the sample was cooled to 5 K in the presence of a field of 100 Oe, and then the magnetization was measured with increasing temperature in the same field. The ZFC and FC magnetization curves are plotted in figure 6 for comparison between two typical dried samples, i.e. one prepared in oleylamine at 215 °C, which has the pure fcc nickel phase, and the other prepared in the mixture of oleylamine and octadecene at 240 °C, which has the pure hcp nickel phase.

As seen from figure 6, a distinct magnetic cooling effect is observed for both samples. For the fcc nickel nanoparticles, the ZFC magnetization monotonically increases with increasing temperature and the FC magnetization almost does not change; the splitting ZFC–FC magnetization curves reach a crossing point around 300 K, indicating a blocking temperature above room temperature. Compared to those fcc nickel nanoparticles with smaller sizes [4, 5, 10], the as-synthesized fcc nickel nanoparticles which have typical sizes of 30–40 nm possess a higher blocking temperature. This can be attributed to the size-dependent properties of blocking temperature. The blocking temperature is related to the size of the magnetic particles and the magnetocrystalline anisotropy constant (K) by the equation $K = 25k_BT_B/V$, where k_B and V are the Boltzmann constant and the volume of a single particle, respectively, and T_B is the blocking temperature. For a spherical particle with a diameter of 34 nm, if the K value of bulk nickel (5×10^4 erg cm^{-3} [25, 26]) is substituted in the equation, the deduced T_B is 298 K.

The ZFC magnetization curve of the hcp nickel sample is quite different from that of the fcc nickel sample, in which a sharp maximum at a temperature around 12–13 K is observed (figure 6(b)). It is worth mentioning that such a sharp maximum at about 12 K (the blocking temperature) has also been observed in recent studies [10, 15] on the magnetic properties of the hcp nickel nanoparticles which have different sizes from those (typical sizes of 35–40 nm) synthesized in our study. This implies that the hcp nickel nanoparticles have a small dependence of the blocking temperature on their sizes. Above the blocking temperature, the magnetizations in both of the ZFC and FC curves of the hcp nickel nanoparticles begin to decrease quickly and reach a value close to zero. This negligible magnetization is also in contrast with that of the fcc nickel nanoparticles.

Hysteresis loops of the fcc and the hcp nickel nanoparticles measured at 5 K are shown in figure 7. Both samples present a hysteretic behavior. The coercivity of the fcc nickel nanoparticles at 5 K is 273 Oe whereas that of the hcp nickel nanoparticles is 891 Oe. The coercivity measured at 300 K for these two samples is basically negligible. On the other hand, however, the magnetization of the fcc nickel nanoparticles increases very quickly and is nearly saturated in a field of 10 kOe, whereas that of the hcp nickel nanoparticles

increases slowly and does not reach a saturation even at a field of 50 kOe. The value of saturation magnetization (M_s) measured at 5 K of the fcc nickel nanoparticles is 53.7 emu g^{-1}, which is rather close to that of bulk fcc nickel, revealing a metallic characteristic. In contrast, the M_s value (11.5 emu g^{-1}) of the hcp nickel nanoparticles is much lower than that of the fcc nickel nanoparticles. Such a difference in the M_s value is further intensified in the results obtained at 300 K, in which the M_s value of the fcc nickel nanoparticles does not decrease much (48.5 emu g^{-1}), whereas that of the hcp nickel nanoparticles is almost close to zero. These observed results indicate that the magnetic properties of the hcp nickel nanoparticles are quite different from that of the fcc nickel nanoparticles.

The differences of magnetic properties between fcc and hcp nickel nanoparticles have also been observed in several recent studies [10, 14, 15, 18]. On the magnetism of hcp nickel nanoparticles, there are several different reported results: nonmagnetic [14], antiferromagnetic [10] and ferromagnetic [18]. Clearly, the nonmagnetic property is not supported by our magnetic measurement data because a sharp peak at a temperature around 12–13 K is observed in the ZFC curve. In addition, the superparamagnetic behavior of ferromagnetic hcp nickel nanoparticles also cannot explain the very sharp peak in the ZFC curve, very small particle size dependence of T_B and nearly zero magnetization above T_B in the M–T curve. Further experiments are needed to clarify the magnetic behavior of hcp nickel nanoparticles.

4. Conclusions

We report the synthesis of nickel nanoparticles via the thermal decomposition of nickel(II) acetylacetonate in several important alkylamines, including oleylamine, trioctylamine, dodecylamine and hexadecylamine. The alkylamines serve as both solvents and reducing agents and no additional reducing agents are needed in the reaction systems. Such a synthetic protocol is relatively simple and effective, and is possible to extend to other metal systems. By choosing appropriate reaction temperature and solvent, nickel nanoparticles that have the fcc or the hcp phase can be obtained. The formation of the hcp phase seems to favor a higher reaction temperature in these alkylamines. The particle size distribution and morphology were further controlled by introducing surfactants (oleic acid and trioctylphosphine) and monodisperse nickel nanoparticles were successfully obtained. The results of magnetic characterization showed that the hcp nickel nanoparticles exhibited quite different magnetic properties from those of the fcc nickel nanoparticles. The observed magnetic behavior of the hcp nickel nanoparticles is rather complex and further work is needed to elucidate the magnetic behavior of the hcp nickel nanoparticles.

Acknowledgments

This work was partially supported by the Natural Science Foundation of Fujian Province of China (no. 2006J0172), the National Natural Science Foundation of China under grant no. 50671087 and the Start-up Foundation of Xiamen University. We thank the Center for Nano-Science and Technology, Xiamen University for use of the TEM facilities.

References

[1] Edelstein A S and Cammarata R C 1998 *Nanomaterials: Synthesis, Properties and Applications* (Bristol: Institute of Physics Publishing)
[2] Petit C, Taleb A and Pileni M P 1998 *Adv. Mater.* **10** 259
[3] Toshima N and Yonezawa T 1998 *New J. Chem.* **22** 1179
[4] Murray C B, Sun S, Doyle H and Betley T 2001 *MRS Bull.* **26** 985
[5] Hou Y and Gao S 2003 *J. Mater. Chem.* **13** 1510
[6] Green M and O'Brien P 2001 *Chem. Commun.* 1912
[7] Bradley J S, Tesche B, Busser W, Maase M and Reetz M T 2000 *J. Am. Chem. Soc.* **122** 4631
[8] Chen D H and Hsieh C H 2002 *J. Mater. Chem.* **12** 2412
[9] Chen L, Chen J, Zhou H, Zhang D and Wan H 2007 *Mater. Sci. Eng.* A **452/453** 262
[10] Jeon Y T, Moon J Y, Lee G H, Park J and Chang Y 2006 *J. Phys. Chem.* B **110** 1187
[11] Jeon Y, Lee G H, Park J, Kim B and Chang Y 2005 *J. Phys. Chem.* B **109** 12257
[12] Toneguzzo P, Viau G, Acher O, Guillet F, Bruneton E, Fievet-Vincent F and Fievet F 2000 *J. Mater. Sci.* **35** 3767
[13] Hinotsu T, Jeyadevan B, Chinnasamy C N, Shinoda K and Tohji K 2004 *J. Appl. Phys.* **95** 7477
[14] Chinnasamy C N, Jeyadevan B, Shinoda K, Tohji K, Narayanasamy A, Sato K and Hisano S 2005 *J. Appl. Phys.* **97** 10J309
[15] Tzitzios V, Basina G, Gjoka M, Alexandrakis V, Georgakilas V, Niarchos D, Boukos N and Petridis D 2006 *Nanotechnology* **17** 3750
[16] Zhang H T, Wu G, Chen X H and Qiu X G 2006 *Mater. Res. Bull.* **41** 495
[17] Park J *et al* 2005 *Adv. Mater.* **17** 429
[18] Han M, Liu Q, He J H, Song Y, Xu Z and Zhu J M 2007 *Adv. Mater.* **19** 1096
[19] Li D S and Komarneni S 2006 *J. Am. Ceram. Soc.* **89** 1510
[20] Ely T O, Amiens C, Chaudret B, Snoeck E, Verelst M, Respaud M and Broto J M 1999 *Chem. Mater.* **11** 526
[21] Cordente N, Respaud M, Senocq F, Casanove M J, Amiens C and Chaudret B 2001 *Nano Lett.* **1** 565
[22] Leng Y, Zhang Y, Liu T, Suzuki M and Li X 2006 *Nanotechnology* **17** 1797
[23] Yamamoto M, Kashiwagi Y and Nakamoto M 2006 *Langmuir* **22** 8581
[24] Hiramatsu H and Osterloh F E 2004 *Chem. Mater.* **16** 2511
[25] Bala T, Bhame S D, Joy P A, Prasad B L V and Sastry M 2004 *J. Mater. Chem.* **14** 2941
[26] Cullity B D 1972 *Introduction to Magnetic Materials* (Reading, MA: Addison-Wesley)